Ship performance monitoring dedicated to biofouling analysis: development on a small size research catamaran

Alessandro Carchen[a]*, Mehmet Atlar[b], Serkan Turkmen[a], Kayvan Pazouki[a], Alan J. Murphy[a]

[a]*School of Engineering – Marine, Offshore and Subsea Technology Group, Newcastle University, Newcastle upon Tyne, UK;* [b] *Department of Naval Architecture, Ocean and Marine Engineering, Strathclyde University, Glasgow, UK*

*corresponding author: a.carchen@newcastle.ac.uk

This paper provides a description of the deterministic ship performance monitoring system developed and installed on Newcastle University's Research Vessel, *The Princess Royal*, for the estimation of the effect of hull and propeller fouling on the vessel's performance. The study revolves around the principle of data normalisation, both in its theoretical and practical aspects. A procedure for correcting weather and operational disturbances is introduced that takes into account plausible resources limitations. According to the needs emphasised by the normalisation process, the required onboard measurement system is described as it was implemented on the research vessel. A robust method to prepare the raw data for the analysis and suitable for all ship types and sizes is then proposed. A performance analysis method is finally defined using four different indicators of the vessel hydrodynamic performance. On-board measurements are presented and analysed according to the proposed methodology. Results show an increase in resistance of over 20% with extensive shell fouling and prove the effectiveness of the used method.

Keywords: biofouling; ship performance monitoring; ISO 19030; hull roughness; marine propulsion; frictional resistance.

1 Introduction

The growth of biofouling on ship hulls has always been a great concern for shipping due to its fast advancement and the predicament of its prevention and removal. Predictions of penalties due to biofouling growth on ship hulls reach in the worst-case 80% of the

nominal shaft power in the presence of heavy calcareous fouling [1]. Such circumstances can be avoided if a good fouling control system is adopted, and the progress of fouling penalties are observed with a suitable ship monitoring plan. The modern Ship Performance Monitoring System (SPMS) is rooted in the renowned study conducted by Telfer [2], who showed that the analysis of service performance could be used for the detection of fouling. However, since the effect of fouling on vessel performance is not directly measurable, distinguishing it from the effects caused by other phenomena (e.g. wind, waves) is one of the greatest challenges in full-scale measurements. The success of tackling this challenge thus chiefly depends upon the availability of quality measurements and on the technique used to analyse them.

Whereas recent environmental regulations are making performance monitoring a necessity rather than just a beneficial option (e.g. [3,4]), on the other hand, the market of fouling control using coatings offers plenty of solutions [5,6]. In this framework, SPMSs remain the primary aid in the assessment of a fuel management strategy, of the effectiveness of a new retrofit and the evaluation of different coating systems on the short and long terms. Hence, the interest in Ship Performance Monitoring recently has paved the way for the introduction of the ISO 19030 [7], the first standard dedicated to the analysis of hull and propeller performance.

Despite the well-established use of SPMSs, however, the research in this field is far from being exhausted because of the following reasons:

1. the complexity of the ship's operating conditions and the lack of analytical solutions to several of the problems they imply (e.g. influence of the seaway, effect of drift motions and currents, etc.);
2. the development of commercially owned SPMSs, often confidential or dependent from the service beneficiaries;

3. the rapid advancements of computer and sensors technologies, permitting superior data acquisition, quality and analysis.

This research is thus conducted in the attempt to provide an independent Ship Performance Monitoring System, dedicated to the analysis of biofouling growth on hull and propeller and to be an instrument in the selection of a suitable fouling control system in retrospective. In achieving this aim, a transparent, physics-based approach is employed, whose benefits against other available methods are discussed. In the attempt to clarify and generalise some aspects of Performance Monitoring (e.g. data handling and correction techniques) that are simply assumed 'as-is' by most applications, a detailed investigation is carried out on all the data treatment stages. The proposed methodology is implemented and tested on Newcastle University's Research Vessel (R/V), *The Princess Royal*, proving to be one of the few applications of a Ship Performance Monitoring System on small-size vessels. Regardless, the method presented in this paper can be applied to any vessel whose operator's intention would be to assess the effect of a fouling control coating application or that of biofouling build-up on the ship's wetted surface and propeller.

Following this introduction of the paper, a review of the current state-of-the-art approaches to ship performance monitoring in support of the adopted choice is given next. Then, the factors affecting ship performance and the method used to correct their effect are described in Section 2. The necessary measurements identified by the data correction process define the characterisation of the onboard measurement system, which is described in Section 2.2. Raw data handling techniques, necessary to pre-process the data before the correction and the analysis, are then discussed in Section 2.3. Reference is always made throughout the paper to the full-scale achievements on board Newcastle University's R/V. The results of ship performance monitoring carried out

over the past year on the R/V are presented and discussed in Section 3 while the conclusions are drawn in Section 4 of the paper.

1.1 Review of current approaches to ship performance monitoring

The variety of performance monitoring solutions available today may be grouped in reason of their data analysis method. Three major streams appear to have evolved that are relevant to contemporary applications - the deterministic, the data-driven and hybrid approaches.

The deterministic approach is the same well-known principle long used for the analysis of sea trials [8], whereby the representation of the ship behaviour is, with the due assumptions, modelled employing physical governing laws and causal relationships between them. When modelling the ship's performance, experimental or numerical techniques are employed to model parts of the total resistance. Depending on the project, employing Experimental Fluid Dynamics (EFD) in the development of a deterministic SPMS might involve the use of towing tank data, cavitation tunnel experiments and wind tunnel measurements. EFD techniques are, however, often complemented or replaced by Computational Fluid Dynamics (CFD). Both methods are ship-specific and very accurate, but they require substantial resources to undertake extensive testing or simulation campaigns. Therefore, their use is usually confined to the assessment of only the propeller open water characteristics and relevant conditions of additional resistance components. For example, CFD may be used to estimate the added wave resistance in head seas, for a specific draught and a limited range of wave frequencies. When the case allows it, semi-empirical methods can be used, for instance to calculate wind resistance coefficients. Care has to be taken, however, in checking the limits of applicability such methods. Several SPMSs based on the deterministic method

can be found in literature, e.g. [9,10,11,12,13].

Data-driven methods do not require any knowledge of the physical phenomena they aim to model since all the data manipulation and statistical analysis is entirely carried out by computers using powerful self-learning (adaptive) algorithms. The derivation of the transfer functions relating one or more measurands (e.g. wind speed and direction) with one or more observed variables (e.g. ship's speed and power) is attained by using pure statistical inference on the measured data. Data-driven methods are therefore also referred to as Black Box models. During the implementation of a data-driven model, a large portion of the available data is used to *train* the model and two smaller portions of data are used to validate it and test it. Data-driven methods in the relevant literature encompass Artificial Neural Networks [14], Gaussian Processes [15], Multivariate Adaptive Regression Splines [16], Genetic Algorithms [17] and Random Forest [18].

Hybrid methods implement the same statistical tools used by data-driven methods, but using some simplified physical knowledge to supervise their development. Hybrid approaches are thus also known as Gray models. These methods generally use a simple underlying physical model (e.g. Holtrop's regression for the ship resistance) that is then refined by the analysis of historical on-board measurements, accomplished using any of the data-driven techniques earlier presented [18]. Examples are described in [16,19,20,21,22].

Despite being able to achieve comparable accuracy, all three of these categories have benefits and drawbacks, and all require relevant expertise to be built. The data-

driven methods can be very accurate even in the prediction of non-linear problems and are relatively inexpensive, but they are as accurate as the measured data from which the models are developed. On the other hand, these methods normally need several months of onboard recorded data [16]. Also, tuning the statistical parameters to avoid model overfitting is a challenging task that requires expertise to be performed [18]. Hybrid methods are superior to the data-driven methods because the base physical knowledge they retain acts as a constraint for the data-driven technique used to analyse the measurements history. Nevertheless, the accuracy of both methods is good only within the boundaries of their training data set [18]. Moreover, they heavily rely on the on-board data quality, consistency and variety. Data variety, in particular, is often the most challenging to obtain since ships normally sail at a fixed RPM, power or speed. The major consequence is that the data-driven and hybrid models may suffer from multicollinearity and variable confounding [16]. On the other hand, accurate deterministic methods may require, in various degrees, a reasonable investment of resources and technical information that is at times not easily accessible. However, deterministic methods can be used immediately after their onboard implementation and are more suitable than the other two methods for the analysis of onboard measurements collected over shorter periods [16]. By definition, deterministic methods are also transparent. Thus the model and all the data used can be inspected, validated and 'extracted' at any time. Therefore, it is possible to utilise the deterministic SMPS itself to validate sub-models, to provide feedback to earlier designs, to verify performance predictions, and to obtain additional physical information to aid further design or operational investigations. Since the accuracy of the deterministic methods does not change over time, they are also suitable for long term studies, such as fouling assessment on ship hulls, thus widening the scope of their possible applications, e.g.

long term monitoring, short-term retrofit analysis [23], validation of other performance prediction techniques [24].

Within the above framework, despite the economic advantages often fostered by the data-driven or hybrid methods, a deterministic method is preferred in this study.

2 Methodology

Changes in wetted surface roughness of a vessel alter the boundary layer of the hull and hence its viscous drag. However, the complex environmental and operational profile of a ship also introduces additional resistance components that need to be inspected before investigating the effects of biofouling on the ship's performance. This raises the need to define a *reference* sailing condition against which to assess in-service performance data. For convenience, the reference sailing condition is identified by the clean hull and calm weather at one or more loading conditions of the vessel. In virtue of the superposition principle, the total in-service resistance R_T of a vessel may then be described as:

$$R_T = R_v + R_w + R_{add} \tag{1}$$

where R_v is the viscous drag, R_w the wave pressure resistance and R_{add} the added resistance caused by external disturbances (eg loading condition, wind, waves etc.). The effect of a change in the hull surface roughness caused by fouling is negligible on all resistance components but the viscous drag. A simple representation of the ship resistance with fouled hull may then be:

$$R_T = (1 + \phi)R_v + R_w + R_{add} \tag{2}$$

where ϕ shall be termed fouling coefficient and represents the effect of fouling on the viscous resistance of the ship. Some important aspects related to ship resistance need to be considered, described as follows:

1. The analysis here presented is a relative assessment of parameters measured under different hull roughness. In this perspective, the absolute accuracy of the measurements assumes secondary importance compared to their consistency over time.
2. Deterministic approaches substantially employ two ways to minimise the impact of R_{add}, namely data filtering and data correction. Data correction procedures attempt to eliminate R_{add} by correcting the measured data to ideal conditions – much in the same way as during the analysis of speed-power trials [8]. According to the ISO 19030, this process is also called *normalisation* [7]. Filtering techniques instead attempt to minimise R_{add} by discarding all measurements conducted with environmental and operational conditions outside pre-defined ranges (i.e. too `far' from the ideal conditions). This includes conditions that cannot or should not be corrected for. Data filtering is carried out prior to the normalisation stage during the data *preparation* [7]. When assessing the ship performance using these methods, it is customary to use a blend of filters and corrections [7,8]. Regardless, the weaknesses of both ought to be known. Excessive filtering typically diminishes the quantity of data suitable for the analysis, weakening the derived statistics. Excessive correction, on the other hand, may lead to an increase in the data noise if corrections are applied outside of their domain of applicability or if they are simply not accurate.
3. Since ship resistance is not directly measurable, the propulsion power stands as its closest proxy, which can be represented as:

$$P_S = \frac{T_p V_s}{\eta_0 \eta_r \eta_s}(1 - w) \tag{3}$$

where P_S is the measured shaft power, T_p the propeller thrust, V_s the ship speed through the water, w the Taylor wake fraction and η_0, η_r, η_s respectively the open water, relative rotative and shafting efficiencies. Filtering and normalization techniques ought to consider alterations of both the ship speed and the effective wake.

Based on the above considerations, a deterministic SPMS was developed and implemented on the 18m catamaran *The Princess Royal*. Table 1 reports her principal particulars.

[Table 1 here]

The reference coordinate system is shown in Figure 1. The axis x_0 and y_0 lay on the still water surface, o coincides with the midship, u and v_m are the axial and normal components of the total ship speed through the water V_s on the ship axis system and β, ψ, δ the drift, heading and rudder angles respectively. In the paper, reference is made length-based Froude number F_n defined by:

$$F_n = \frac{V_s}{\sqrt{L_{oas}\, g}} \tag{4}$$

where $g = 9.807$ m s^{-2} is the gravitational acceleration and L_{oas} is the length overall submerged.

[Figure 1 here]

Figure 2 summarises the performance monitoring process that will be described in the following sections, showing the data flow through the complete SPMS, from the onboard measurements to the derivation of in-service performance. Nevertheless, since the method to correct the disturbance determines the measurements that are required from the onboard system, the next section begins with an investigation about the

possible correction procedures. A presentation of the measurement system will then be given, and followed by an analysis of the raw data handling method. Finally, the proposed performance analysis method is presented.

[Figure 2 here]

2.1 Normalisation of disturbances

In the following, the methods used to normalise the effects of disturbances on ship performance are presented under the assumption of constant sailing speed and heading. The principle of superposition is adopted since the correlation between disturbances can be neglected if the effects of disturban ces are not large [8].

Waves

The effect of waves is challenging to evaluate due to its complexity and the difficulty of obtaining accurate measurements of the encountered seaway. Waves produce added resistance and affect the propeller wake. Added wave resistance is greater for bow waves, and is higher in the bow quarter for most hull forms [25]. Stern quartering and following seas cause smaller added resistance but can alter the propeller inflow significantly (up to 10% according to [26]). Induced drifting, yawing and steering produce additional resistance components that will be discussed separately. The time-averaged added wave resistance in irregular waves can be described as [27]:

$$\bar{R}_{AW} = 2 \int_0^{2\pi} \int_0^{\infty} \sigma_{AW} \, S_\zeta \, \mathrm{d}\omega_e \, \mathrm{d}\psi_\zeta \tag{5}$$

where S_ζ is the directional wave spectrum, σ_{AW} the mean nondimensional added wave resistance transfer function in regular waves, ω_e the wave encountering frequency and

ψ_ζ the relative wave direction. σ_{AW} is not simple to predict, particularly for unconventional hulls, in beam and quartering seas and at low Froude numbers [28]. According to the Author's research, the use of modern numerical panel methods or advanced modified strip theories limited to head waves predictions, complemented by the application of a directional filter is a sensible and practical choice that improves the data quality and requires limited resources [29]. Other conditions, including those where strong non-linear effects become prominent (e.g. slamming), must be filtered out. Where other and more comprehensive means (e.g. seakeeping tests, CFD etc.) can be used, they shall be employed as per their availability. On the other hand, the effect of waves on ship wake is not simply estimated and it is recommended to avoid correcting for it by applying suitable filters instead. The application of a directional filter allows for the following, stern quartering and bow quartering seas to have stricter filtering, while the beam seas to have more relaxed thresholds. To reflect this, a simple directional filtering criterion can be devised in the form:

$$H_S \leq \begin{cases} H & \text{if } 160^\circ < \psi_\zeta < 200^\circ \\ H\left[1 + k_h \cos^2\left(\psi_\zeta\right)\right]^{-1} & \text{Elsewhere} \end{cases} \quad (6)$$

where $H = 2.25\sqrt{L_{pp}}/100$ is the ITTC total significant wave height threshold when the encountered wave spectrum is measured [8]; $\psi_\zeta = 180^\circ$ identifies the head waves; k_h is a filter strictness parameter. A suggested value of $k_h = 0.5$ reduces the bow and stern allowed wave height by a third and the added wave resistance and the wake fraction change by about half.

Head waves σ_{AW} was calculated for *The Princess Royal* by means of a numerical code employing Faltinsen's $2^{1/2}$D high-speed theory [30]. The simulations were validated using towing tank test results, presented in the Appendix [31]. Because the loading condition of the R/V varies but slightly, only one displacement was used in the analysis. Due to her seakeeping characteristics, to avoid wetdeck slamming and the consequent nonlinear response to the incident waves *The Princess Royal*'s significant wave height threshold H of eq. (6) was reduced to:

$$H = 0.55 \text{ m} \tag{7}$$

Winds

Winds exert on a vessel a direct resistance and an indirect resistance due to drift, yaw and steer to keep the course. The direct wind resistance can most accurately be derived using relatively simple CFD simulations or wind tunnel tests. Systematic experiments and regressions are also available in the literature for certain common ship classes [32,33,34], but the shape and superstructures must be very carefully assessed against that of the database. The time-averaged direct wind resistance is defined:

$$\bar{R}_{AA} = 0.5\, \rho_a\, U_{AAR}^2\, C_X(\psi_{AAR}) L_{oa}^2 \tag{8}$$

where ρ_a is being the air density, U_{AAR} the relative wind speed and C_X the wind resistance coefficient in surge direction, the function of the relative wind direction ψ_{AAR}. *The Princess Royal*'s wind resistance coefficients were derived by wind tunnel tests and CFD simulations as reported by [35]. Equation (7) is constraining on the wind in the majority of the weather conditions and corresponds to Beaufort 3 approximately. However, at the onset of a strong wind waves may not have formed yet to produce a reasonable monitoring threshold for wind. Thus, the ITTC [8] wind threshold of 10m/s

shall be used as an upper wind speed limit. The indirect wind resistance will be treated separately in the following paragraphs.

Drift, yaw and steering

Figure 2 shows the relations between the vessel and water surface motion. The drift of the vessel over the ground may be practically considered as made of two components, namely the leeway drift (a) and the surface current drift (b). Provided that a good measurement of the speed through the water V_s is available, only a is relevant because it alters the water flow around the hull and propeller. Drift motion is often complemented by yaw motions due to the unbalanced hydrodynamic side forces and steering to keep the intended course.

[Figure 2 here]

Drift and yaw produce coupled resistance components on the hull, which in manoeuvring terms can be expressed as:

$$R_{\beta,\dot{\psi}} = 0.5\rho L_{pp} T V_s^2 \left(X'_{\beta\beta}\beta^2 + X'_{\beta\dot{\psi}}\beta\dot{\psi} + X'_{\dot{\psi}\dot{\psi}}\dot{\psi}^2 \right) \quad (9)$$

where T is the midship draft and β and $\dot{\psi}$ are the drift angle and yaw rate respectively. Whilst the latter can be easily measured, e.g. with a gyrocompass, the former requires the measurement of the transverse speed the through water v_m, obtained only from dual axis speed logs. $X'_{\beta\beta}, X'_{\beta\dot{\psi}}$ and $X'_{\dot{\psi}\dot{\psi}}$ are the manoeuvring hydrodynamic derivatives, whose estimation can be accurately obtained by conducting manoeuvring tank tests [36] or complex CFD simulations, both of which require however significant resources. Semi-empirical formulas can be found in the literature to estimate the hydrodynamic derivatives, but the utmost care must be taken in the use of these formulae due to the sensitivity of $R_{\beta,\dot{\psi}}$. The simulation of a simple course-keeping zig-zag manoeuvre with

maximum rudder angle of 5 deg conducted on a small cargo vessel [37] shows that $R_{\beta,\dot{\psi}}/R_T \approx 0.03$ in calm waters for $\beta \approx 3$ deg and $\dot{\psi} \approx 0.2$ deg/s.

According to many manoeuvrability models, the steering resistance depends on the rudder force. However, the correct estimation of the rudder inflow velocity is not in the least easy, and it involves the use of several experimental constants. Manoeuvrability simulations can again demonstrate that the lack of a good estimation of the rudder inflow leads to errors in the steering resistance of over 30%. On the other hand, it can also be shown that for the same course-keeping manoeuvre presented above, $R_\delta/R_T \approx 0.03$. Because *The Princess Royal* couldn't be fitted with a dual axis speed log and no good estimation of the rudder inflow could be obtained, no correction was applied for either the drift and steering resistance. Excessive drifting motion of the vessel can be approximately detected in this case by looking at the over-ground drift angle and the rudder usage [11]. The ISO 19030 approximate filtering criteria are thus used to limit the impact of drift, yaw and steering [7]:

$$\max|\psi - \psi_g| = 3 \text{ deg} \tag{10a}$$

$$\max|\delta| = 5 \text{ deg} \tag{10b}$$

Finally, drift and yaw motions also contribute substantially to alter the wake field in front of the propeller. An accurate estimation of such changes is very difficult, although several empirical equations have been derived, e.g. in [38]. Within the constraints of Eq. (10), however, the change of effective wake fraction can be neglected.

Shallow waters

Speed corrections for restricted waters are possible using the methods by Lackenby [39] or the more recent by Raven [40]. However, while these are valid only for a few

geometric families of hulls, speed correction for shallow waters should be avoided by discarding all measurement conducted in areas where the water depth is less than [8]:

$$h = \max\left(3\sqrt{BT}, 2.75\frac{V_s^2}{g}\right) \quad (11)$$

which corresponds to $h = 28$m in the present case.

Changes in water properties

According to the ITTC [8], the effects of changes in water density ρ and kinematic viscosity ν are calculated:

$$R_\rho = R_{T0}\left(1 - \frac{\rho}{\rho_0}\right) - R_f\left(1 - \frac{C_{f0}}{C_f}\right) \quad (12)$$

where C_f and C_{f0} are the frictional resistance coefficients for actual and reference water properties respectively; R_{T0} is the total resistance in reference waters; R_f is the frictional resistance in actual waters; ρ and ρ_0 are the water densities respectively in actual and reference conditions (15°C and density of 1025 kg m). The resistance coefficients are described as customary i.e.:

$$C_f = \frac{R_f}{0.5\rho S V_s^2} \quad (13)$$

where S is the wetted surface area. The effect of a change in water density is generally small considering the negligible worldwide variation of ρ [11]. In the case of *The Princess Royal*, R_ρ accounts for about 0.5% of the total resistance in the worst case scenario.

Change of loading condition

For changes in displacement of up to 5% of the reference value, the change in wake

field is negligible and the change in resistance can be estimated by the well-known relation [7,8]:

$$R_\Delta = \left[1 - \left(\frac{\Delta_0}{\Delta}\right)^{\frac{2}{3}}\right] R_T \quad (14)$$

where R_Δ is the resistance increase due to displacement change, Δ_0 is the reference displacement and R_T the measured total resistance. For greater changes in displacement, the interpolation from model test data or CFD results is instead recommended [8]. In this study, the change in displacement, corresponding to a displacement change of about 2 tonnes, affected the powering of the R/V by about 3%. Apart from the employment of CFD simulations, no reliable correction exists to date for trim changes, whose effect was thus neglected.

Normalisation procedure

The normalisation procedure used in this research is based on the speed and torque identity method proposed by Taniguchi and Tamura [41] for the analysis of sea trials. The main assumption of this method is that in steady-state conditions and at ship speed V_s, the full-scale propeller operating in a velocity field with effective wake fraction w delivers the same thrust as in open water condition under the speed $V_s(1-w)$. The open water characteristics of the propeller relate the propeller thrust with torque and allows the calculation of the propeller efficiency. Since thrust is a less reliable measurement than torque, propeller open water curves allow to indirectly measure thrust by measuring torque. Open water tests for *The Princess Royal*'s propellers were conducted at Newcastle University's Emerson Cavitation Tunnel [23]. Where experiments wouldn't be possible, reliable alternatives (eg vortex lattice models, surface panel methods, CFD etc.) can be used to calculate the propeller's open water

characteristics based on its geometry. An estimate of the thrust deduction factor also needs to be made, despite a high accuracy is not essential for this parameter. Self-propulsion tests for the R/V were carried out at Istanbul Technical University [42].

The normalisation procedure is here described. The measured propeller coefficients are defined from:

$$K_Q = \frac{Q_p}{\rho n^2 D_p^5}\eta_r\eta_s \tag{15a}$$

$$K_T = \frac{T_p}{\rho n^2 D_p^4} \tag{15b}$$

where Q_p and n are the measured propeller shaft torque and speed respectively. The efficiencies were estimated $\eta_r \approx 1$ and $\eta_s = 0.98$. For convenience, both propeller coefficients are expressed as second-order polynomials of the propeller coefficient of advance J:

$$K_Q = \mathrm{f}(J) = a_0 + a_1 J + a_2 J^2 \tag{16a}$$

$$K_T = \mathrm{g}(J) = b_0 + b_1 J + b_2 J^2 \tag{16b}$$

As reported, e.g. by Mosaad [43], fouling affects the propeller torque and only negligibly its thrust. On the other hand, thrust measurements tend to be less consistent and exhibit more scatter than torque. Therefore, the measured thrust is suggested for use in later stage analysis only, whereas torque is instead used as the primary performance measurement. Hence, two separate J numbers are calculated, one based on the measurement of torque and one based on the measurement of thrust (when available):

$$J_Q = \mathrm{f}^{-1}(K_Q) \tag{17a}$$

$$J_T = \mathrm{g}^{-1}(K_T) \tag{17b}$$

The thrust coefficient is recalculated from J_Q using eq. (16) as:

$$K_{T_{KQ}} = \mathrm{g}(J_Q) \tag{18}$$

It should be noted that in reference conditions and no propeller fouling $K_T = K_{T_{KQ}}$, but not necessarily so in any other case. The full-scale effective wake fraction is calculated according to both advance coefficients of eq. (17):

$$w_Q = 1 - \frac{nD_pJ_Q}{V_s} \tag{19a}$$

$$w_T = 1 - \frac{nD_pJ_T}{V_s} \tag{19b}$$

and an apparent wake fraction can be defined as:

$$w_{app} = w_Q - w_T \tag{20}$$

The function of the apparent wake fraction will be described in Section 2.4. The propeller loading point is defined by:

$$\tau = \frac{K_{T_{KQ}}}{J_Q^2} \tag{21}$$

The total measured resistance is thus estimated from the following equation:

$$R_T = \rho D_p^2 V_s^2 (1 - t_d)\left(1 - w_Q\right)^2 \tau \tag{22}$$

where ρ is the water density, D_p the propeller diameter, V_s the ship speed through water, t_d is the thrust deduction factor and w_Q the torque-derived wake fraction.

Recalling that in this study the manoeuvring resistance $R_{\beta,\dot{\psi}}$ and the steering resistance R_δ are neglected, the total added resistance of eq. (1) is calculated as:

$$R_{add} = \overline{R}_{AA} - \overline{R}_{AA0} + \overline{R}_{AW} + R_{\Delta} + R_{\rho} \tag{23}$$

where $\overline{R}_{AA0} = 0.5\rho_a V_g^2 C_X(0) L_{oa}^2$ is the time-averaged air resistance [11]. The correction of the propeller loading condition is thus carried out accordingly:

$$\tau_0 = \tau - \Delta\tau \tag{24}$$

with

$$\Delta\tau = \frac{R_{add}}{R_T}\tau \tag{25}$$

The corrected (or normalised) propeller advance coefficient and torque coefficients are calculated from:

$$J_{Q0} = \frac{-b_1 - \sqrt{b_1^2 - 4b_0(b_2 - \tau_0)}}{2(b_2 - \tau_0)} \tag{26}$$

$$K_{Q0} = \mathrm{f}(J_{Q0}) \tag{27}$$

Accordingly, the normalised propeller speed can be calculated from:

$$n_0 = \frac{J_Q}{J_{Q0}} n \tag{28}$$

Finally, the normalised delivered power can be calculated as:

$$P_{D0} = 2\pi\rho D_p^5 K_{Q0} n_0^3 \eta_s \tag{29}$$

2.2 Measurement system

The considerations made in the previous section provide the requirements for the measurement system to be implemented on board. In the past, measurements were exclusively taken by manual noon reports, prone to several inaccuracies caused by

human errors in addition to those of the sensors. The great advantages of modern automated acquisition systems have been experienced by the authors and proven in the relevant literature, e.g. [44,45,46]. Quality and quantity are clearly improved by automated systems, and although noon reports are still being used for performance monitoring [47], most ships are now bound to adopt automatic measurement systems by the international regulations [48]. The work of Hasselaar [11] is recommended for a comprehensive discussion on the measurement system quality.

In an automated measurement system, the selection of the sampling frequency is fundamental to obtain the necessary resolution of the observed phenomena. This is particularly important for every parameter depending upon the ship response to disturbances (e.g. V_s). The smaller the vessels are, the higher will be the frequency of their responses and thus the required sampling frequencies. A sampling frequency of 1 Hz provides in general an excellent resolution in most cases.

An automated measurement system was implemented on board the R/V with the sensors described in Table 2.

[Table 2 around here]

[Figure 3 here]

Fig. 3 presents an impression and pictures of the onboard SPMS. To accomplish an accurate speed through the water measurement, a Doppler speed log (a) was installed on the inner side of the starboard demi-hull, around midship. Equation (9) suggests the use of a dual axis log to provide both u and v_m to identify drifting states. However, only a single-axis Doppler Log could be installed on the R/V. In this case, eq. (10a) is used to detect drift. The greatest advantage of the Doppler logs stems from their measurement capability outside the ship's boundary layer (2 m below the keel on the R/V), which makes them unaffected by biofouling and general roughening of the wetted

surface. Contrary to the vast majority of literature statements, Doppler logs deliver accurate and consistent measurements. The majority of the errors imputed to the Doppler logs are related to disturbances to the propeller wake, to stratified ocean currents and to leeway drift. To avoid such elements to influence the vessel's performance, detection strategies similar to those presented in eq. (10) need to be implemented. This was confirmed by an extensive full-scale monitoring campaign lead by MARIN within the joint industry project SPA-TOO, whose outcomes are partly presented in [34]. Measurements can also be affected by heavy pitch motions (over ± 10 deg), by water temperature and by large changes of salinity. Whereas severe heave is avoided with the constraints of eq. (6), the automatic correction of measurements for water temperature changes is a standard on most sensors. Salinity can be assumed almost constant in the range of operations of the R/V, but slight measurement drifts should however be expected in vessels sailing in waters boasting large differences in quality.

Two in-house built instrumented shafts (b) were installed on both shaft lines. Torque and thrust are measured by Wheatstone bridges mounted on two removable shop-calibrated intermediate shafts. A dependence of thrust from torque (a so-called 'parasitic load') was observed during the shop calibrations of the instrumented shafts. This was corrected for in the post-processing phase as explained in the following sections.

Wind speed, direction and properties (density, pressure, temperature etc.) is accomplished using a state-of-the-art onboard weather station (c). The station boasts an ultrasonic anemometer and an array of sensors to measure the air characteristics. To avoid shadowing the anemometer with the ship's superstructure, the location of the weather station is at the highest point of the vessel's mast [49,50]. A check on the

calculated true wind speed over reciprocal runs during acceptance sea trials is a useful assessment in this sense. The measured wind speed needs then to be corrected for the natural wind profile according to the following equation [8]:

$$V_{AAR}(z_{\text{ref}}) = V_{AAR}(z)\left(\frac{z_{\text{ref}}}{z}\right)^{\frac{1}{7}} \tag{30}$$

where $V_{AAR}(z)$ is the relative wind speed measured at the anemometer height $z = 7.55\text{m}$ and $z_{\text{ref}} = 3\text{m}$ is the wind tunnel tests reference height.

The rudder angle is measured using two rudder angle potentiometers located on the rudder stocks (d) and connected to the autopilot. Accurate rudder angle readings help to detect drifting motions and excessive yaw rates.

The solution to Eq. (5), requires knowledge of the wave spectrum S_ζ, which can be measured by specialised wave radars. Due to her limited operational range, a unidirectional vertical wave radar (e) was fitted to *The Princess Royal*, which allows direct comparison of the wave height with the more comprehensive hindcast data of a fixed oceanographic wave buoy located in the operational area.

Because each sensor onboard communicates with a different protocol and sampling frequency, a bespoke monitoring platform (f) was built using a commercial programming language. The main tasks of the software encompass parsing analogical and digital signals from the sensors, unifying their sampling frequencies to 1 Hz, displaying measurements on the user interface and data logging. Finally, two new concept intelligent volume fuel flow measurement systems (g) were installed on both supply and return lines of the engines to compare power measurements. Table 3 summarises the measured variables and their reliability ranking.

[Table 3 here]

2.3 Raw data handling

Before being normalised, the measured raw data should be subjected to initial quality control to identify steady-state periods and outliers. Therefore, a Steady-State Identification (SSI) technique must be at first used to exclude transient periods from the data analysis. As also suggested by the ISO 19030 [7], the following variables should be used as indicators:

(1) Vessel speed, better if V_s;
(2) Propeller speed;
(3) Shaft torque;
(4) Vessel heading or Course Over Ground.

In the literature, mainly two SSI techniques can be found:

- Spread-based SSIs implement dynamic or pre-determined thresholds to assess the dispersion of a data bin and eventually reject it. Dynamic thresholds may be for instance the natural spread of the steady-state signal, whilst the most used dispersion parameters are the range and the standard deviation. Among these methods is the one proposed by the ISO 19030 [7].

- Regression-based SSIs compare the parameters of a curve fitted to a time series to pre-determined values. Curve fitting up to the 2nd order are common. This method, despite being very intuitive, is however both computationally intense and poorly performing in several cases, for example in the middle of a low-frequency oscillation [51].

Both techniques can be applied to either raw or low-pass filtered (LPF) data. Large use is made, for example, of high-threshold filters (eg exponential filters, moving medians

and moving averages).

Slightly different methods are those based on F-test type statistics, which generally assess the ratio of sequential to local dispersion of exponentially filtered raw data [51]. These methods need some parametric tuning, but they do not require data binning and are not computationally demanding. However, when applied to onboard data, F-type SSIs proved excessively unstable and unfit for a robust indication of steady-state periods. Further investigation is needed to asses its applicability in this field.

The SSI strategy also needs to be devised secure from the influence of outliers. Moreover, if the SPMS is to be implemented on-line, the computational burden and time lag of the data analysis should be kept to a minimum. This leads to consider spread-based SSIs the best option but employing measures of dispersion that accommodate for outliers directly on raw data bins. This technique is very robust; it preserves the natural spread of the measurements and is computationally undemanding. Table 4 presents the pre-defined allowable spread, which is based on the expected signal variability from the average for each variable. In the choice of a robust estimator of spread, the α-trimmed standard deviation, s_α^T, and the Interquartile Range, IQR, proved to be the most efficient and robust. The α-trimmed standard deviation can be defined as the standard deviation of an α-trimmed sample. s_α^T needs then to be standardized to be a consistent estimators of the sample standard deviation s at the normal distribution [52]. Therefore, in the case of s_α^T:

$$\hat{s} = \frac{s_\alpha^T}{\gamma(\alpha)} \tag{31}$$

where:

$$\gamma(\alpha) = 1 - 2\alpha - 2\Phi^{-1}(1-\alpha)\varphi[\Phi^{-1}(1-\alpha)] \tag{32}$$

where Φ and φ are respectively the standard normal cumulative distribution and density functions [52]. Owing to the high trimming ratio of the IQR, the trimmed standard deviation was preferred in virtue of its reduced dullness to tail end scatter, which is relevant for instance at the onset of a transient. A trimmed standard deviation with $\alpha = 5\%$ was found to provide excellent results.

[Table 4 here]

To use either of these estimators of spread, the raw data needs to be subdivided in data bins. Each contains some data points N defined as follows:

$$N = f\epsilon \tag{33}$$

where f is the sampling frequency and ϵ a time constant. Since the majority of the existing Ship Monitoring Systems operates on large vessels, the practice has indicated that $\epsilon \approx 10 \div 15$ minutes is a fair size for data analysis. This is not so for smaller vessels, whose response to disturbances can be in the order of seconds. Therefore ϵ must be defined as a ship-dependent constant, which is given by eq. (34) while its full derivation is given in Appendix A:

$$\epsilon = \frac{7941\,\xi}{2724+\xi} \tag{34}$$

where the variable ξ is defined:

$$\xi = \frac{\tilde{V}_s^2 \Delta}{\tilde{P}_s k_t} \tag{35}$$

where $\tilde{P}_s$ is the shaft power at the design ship speed $\tilde{V}_s$, Δ is the displacement and k_t an efficiency coefficient that may be generally taken as 0.55. The time constant ϵ can be applied to any vessel size and type. It provides a round figure of the timing of the slower accelerations experienced by a vessel and therefore of the size of the data bin.

Since in the case of *The Princess Royal* $\epsilon = 23s$, eq. (33) demonstrates that a sampling frequency of 1 Hz provides a reasonable sample size in the case of small vessels.

The Steady-State data bins hence obtained can be assumed to be normally distributed. The eventual outliers in the sample are rejected, most commonly (see, e.g. [7,11], using the Chauvenet's criterion, which has a high probability of rejecting non-outlying values (up to 40% [52]). This study employs instead the generalised Extreme Studentized Deviate (ESD) which is essentially the recursive version of the well-known Grubb's test and has higher statistical power in the detection of outliers [52].

Consecutive data bins measured during the same steady-state period and filtered for outliers are aggregated, and the mean, standard deviation and sample size of each are calculated.

2.4 Performance analysis

Once the data is normalised, the vessel performance against fouling can be assessed observing the variability of parameters commonly termed Key Performance Indicators (KPI) [7]. Most of these are derived from propeller-related variables and may thus include the effect of propeller fouling. In case the KPI is affected by propeller fouling, it will be here represented in its 'fouled' state denoted by a circumflex. In this section, four KPIs are suggested.

The first KPI is based on shaft power and describes the change in normalised power over time t with respect to a reference period t_{ref}. For any given V_s, this KPI can be defined as follows:

$$\widehat{P_K}(t, V_s) = \frac{P_{D0}(t, V_s)}{P_{D0\,\text{ref}}(t_{\text{ref}}, V_s)} - 1 \tag{36}$$

where P_{D0} is the normalised delivered power defined in eq. (29). Power-based KPIs are

robust, easy to interpret and encompass the effect of propeller fouling on the total performance [11]. However, they can be somewhat blunt when used to analyse the effect of fouling.

KPIs derived from the analysis of the measured effective wake fraction are more indicative despite their higher sensitivity to the external disturbances. Since it represents a measure of the mean inflow to the propeller, the wake fraction is directly related to the thickness of the hull boundary layer. Furthermore, the analysis of wake-based KPIs is simplified by the almost linear dependence of the wake fraction from the ship speed. Therefore, the second KPI can be defined as the change in effective wake fraction, described as follows:

$$\widehat{w_K}(t, V_s) = \frac{w_Q(t,V_s)}{w_{Q\,\mathrm{ref}}(t_{\mathrm{ref}},V_s)} - 1 \tag{37}$$

It must be noted that Eq. (37) depends on the propeller open water characteristics and the measured propeller torque Q_p, which can significantly be affected by fouling. Hence, in case of a fouled propeller, w_Q will be an overestimation of the true wake fraction because of the increased drag characteristics of the propeller blades and the reduced open water efficiency. $\widehat{w_K}$ shouldn't therefore be interpreted in its absolute meaning but, rather, as a relative indicator of the combined effect of hull and propeller fouling on vessel performance. In any case, such combined effect is usually of interest to the ship operator.

The distinction between hull and propeller contributions to the increase in propeller torque is possible if either thrust or periodical propeller roughness measurements are available with which to correct the open water curves for fouling effect [53,54]. Thrust measurements usually have higher uncertainty but can serve as good indicators of propeller fouling. However, because the thrust measurement can be

inconsistent and can include parasitic loads (as in our case), a calibration of some sort is necessary. A robust way of doing this is to use w_{app} to indirectly evaluate thrust. w_{app} can be easily calibrated during the reference period against the vessel speed through the water. If properly carried out, the baseline apparent wake fraction will be evaluated secure from most non-linear effects of thrust measurements. As thrust is negligibly affected by fouling, the true effective wake fraction w is well approximated by the thrust-identity wake fraction w_T defined in eq. (19):

$$w \approx w_T \tag{38}$$

According to Eq. (20) and (38), we can thus consider the torque-identity wake fraction as:

$$w_Q = w + w_{app} \tag{39}$$

where w_{app} is the apparent component originated by the torque measured on a fouled propeller and used on open water curves not corrected for the propeller fouling. The third KPI can be thus defined as the ratio between the apparent wake fraction increase and the reference torque-derived wake fraction:

$$w_{app\,K}(t, V_s) = \frac{w_{app}(t,V_s) - w_{app\,\mathrm{ref}}(t_{\mathrm{ref}},V_s)}{w_{Q\,\mathrm{ref}}(t_{\mathrm{ref}},V_s)} \tag{40}$$

$w_{app\,K}$ is an indicator of the accumulation of propeller fouling over time and it represents the proportion of w_Q caused by propeller fouling. Thus, $w_{app\,K}$ will be zero with a clean propeller and increase its value as biofouling builds up on the propeller blades.

The fourth and last KPI is related to the increase of hull viscous drag. Recalling eq. (2) in nondimensional terms:

$$C_T = (1 + \phi)C_v + C_w \tag{41}$$

where the viscous drag coefficient is defined as:

$$C_v = C_f(1 + \kappa) \tag{42}$$

where C_f is the frictional coefficient of the equivalent flat plate and κ is the combined viscous interference and form factor for multi-hulls as defined in [55]. Nondimensional coefficients are defined as in eq. (13). The total resistance coefficient, C_T, can be calculated from eq. (22). Since R_T is estimated from Q_p, it may be a slight overestimation of the real R_T due to the effect of the eventual propeller fouling. It shall therefore be written in its spurious form $\widehat{C_T}$. The wave pressure coefficient can be assessed for the clean hull and propeller as $C_w = C_{T\,\mathrm{ref}} - C_{v\,\mathrm{ref}}$. For fast vessels, both the inception of dynamic lift forces at $F_n \approx 0.4$ and the demi-hulls interaction introduce additional non-linearities that challenge the estimation of C_w and of κ. Therefore, C_w is calculated at the higher F_n where the stable dynamic lift forces in this region define a clearer resistance trend [55]. Numerical analyses showed that for *The Princess Royal* case $\kappa = 0.7765$.

Since C_w is expected to remain almost unchanged with fouling, the fouling coefficient ϕ can be used as a KPI. From eq. (41), we can derive the following:

$$\phi(t, V_s) = \frac{\widehat{C_v}(t, V_s)}{C_{v\,\mathrm{ref}}(t_{\mathrm{ref}}, V_s)} - 1 \tag{43}$$

with $\widehat{C_v}(t, V_s) = \widehat{C_T}(t, V_s) - C_w(V_s)$.

Although ϕ would include the effect of propeller fouling on the calculated resistance if the propeller open water curves are not corrected for, ϕ gives a more detailed indication of the effect of fouling growth on viscous and total resistance. ϕ will be zero on a clean

hull and increase with the increase of fouling on the hull and propeller. If the effect of propeller fouling needs to be separated from that of the hull, the thrust measurements may be used as follows. With reference to eq. (17), (18) and (20), the following can be derived:

$$J_Q - J_T = -\frac{V_s}{nD}\, w_{app} \tag{44}$$

and

$$K_{T_{KQ}} - K_T = -\frac{V_s}{nD}\,\frac{dK_T}{dJ}\, w_{app} \tag{45}$$

where dK_T/dJ is calculated in the operational range ($J = 0.40 \sim 0.55$). Using eq. (22), eq. (45) can be rewritten as:

$$C_{v\,app} = -\frac{2nD^3(1-t_d)}{SV_s}\,\frac{dK_T}{dJ}\, w_{app} \tag{46}$$

where $C_{v\,app}$ is the effect of propeller fouling on the estimation of the viscous resistance and can be defined as:

$$C_{v\,app} = \widehat{C_v} - C_v \tag{47}$$

where C_v is the real viscous drag coefficient. For a fouled hull C_v may be expressed as:

$$C_v = C_f(1+\kappa) + \Delta C_f = C_{v\,\mathrm{ref}} + \Delta C_f \tag{48}$$

where ΔC_f is the frictional coefficient increase caused by hull roughness change as defined by the ITTC '78 [56].

From Eq. (43) and (48) it follows that:

$$\Delta C_f = \phi(1+\kappa)C_f - C_{v\,app} \tag{49}$$

or

$$\Delta C_f = \phi(1+\kappa)C_f + \frac{2nD^3(1-t_d)}{SV_s}\,\frac{dK_T}{dJ}\,w_{app} \tag{50}$$

The derived ΔC_f may then be used in comparison with evaluations of C_f from hull roughness measurements. The application of these four KPIs on *The Princess Royal* case study is described in the following section.

3 Results and discussion

The Princess Royal's SPMS was developed based on dedicated sea trials periodically conducted in a known location of the North Sea off the coast of Blyth (55° 09' N, 1° 28' W). The purpose of the dedicated trials is to facilitate faster data acquisition and to compare the SPMS results with those obtained using recognised international sea trials standards (e.g. [8]). The data collected from the dedicated trials were later complemented by the data collected from the remote monitoring during normal service. The sea trial conducted on the 14th November 2017 served as the baseline trial due to the goodness of the weather and the mild fouling state on the hull (a layer of brown slime). All the KPIs subsequently computed must, therefore, be intended relative to this condition. The 2018 measurements were obtained from in-service monitoring and were therefore dependent on the weather and the daily operational profile. Because of the small size of the vessel, the effect of weather is relatively large and only two days' worth of data could be used during the monitoring period. An underwater inspection carried out on the 13th July 2018, documented a significant growth of fouling on the underwater hull, with widespread heavy slime, some weed fouling and calcareous fouling. The propeller blades were lightly covered by hard slime only (see appendix). The subsequent drydocking (31st August 2018) showed significant calcareous

biofouling (mainly tubeworms) covering both demi-hulls apart from the bow and skeg region (Fig. 5). Considerable algal fouling can be seen to have affected the propellers, particularly the starboard one.

[Figure 5 around here]

Measurements of the normalised in-service delivered power are consistent with the baseline power during the 2017 sea trials and show clear signs of increase during the 2018 in-service monitoring and trials. This is particularly evident at higher speeds, beyond the resistance `hump' typical of semi-planing vessels, while at lower F_n the data scatter is much larger. This reflects the greater uncertainty caused by the relatively heavier impact that the disturbances and shaft residual stresses have on the performance at lower speeds [57]. Because of the 'hump' and the smaller uncertainty, the baseline fit can be determined with greater accuracy for speeds in excess of $F_n = 0.5$. Therefore, only measurements at $F_n > 0.5$ will be here considered in detail.

Figure 6 shows an average $\widehat{P_K}$ of about 19% in July and 24% in August. The corresponding average increases in C_{T0} are 18% (July) and 21% (August). Both indicators are coherent with the amount of fouling despite the relatively short out-of-dock time.

In Fig. 7, the wake fraction gain KPI, $\widehat{w_K}$, shows a general increase in the effective wake fraction, indicating that the inflow to the propeller is slower than the reference value and corroborating the suggestions of the earlier KPI. The variability exhibited by the wake fraction is to be attributed primarily to the higher uncertainty of the speed through water measurements and in the second instance to eventual small waves that caused surface speed fluctuations perceived by the propeller but not by the speed log, which measures at a depth of almost 4m below the water surface. In fact, within the constraints defined in the previous sections, the effective wake is only

partially affected by external disturbances. On the other hand, correcting for all disturbances is not always possible or convenient and therefore some weather or operational effect will always contribute to a limited extent to noise in performance data, where waves are usually the greater contributor. Over the longer term, this high frequency noise would become less relevant with respect to the slower evolving trend of the KPIs.

Because of the similar fouling state of both demi-hulls and propellers and hence wake fractions, the wake KPIs of starboard and port side were averaged in a single value. Under these conditions, the wake fraction gain in Fig. 7 could confirm, with average gains of 25% (July) and 37% (August), both the growth of the hull's boundary layer and the presence of propeller fouling. The apparent wake fraction gain, $w_{app\,K}$ shown in Fig. 8, indicates the fraction of w_Q which is caused by the propeller fouling from the baseline measurement. The plot suggests that by July an average 7% of w_Q is caused by propeller fouling and by August the percentage rises to 36%. The cause of the scatter of $w_{app\,K}$ was investigated to be due to the instability of the strain gauge measurements of the propeller thrust and the cross-correlation with torque. It is interesting to note that the sudden rise in August of $w_{app\,K}$ is coherent with the sudden spread of algal fouling on the propeller blades (see Appendix).

The fouling coefficient ϕ in Fig. 9 estimates average viscous drag increases of 56% (July) and 69% (August). If this is corrected using the information given by the propeller thrust, ΔC_f can be estimated as presented in Fig. 10, which is of an average 2×10^{-3} in both days. The analysis shows that at the time of drydocking ΔC_f had not changed significantly from the previous month and that the additional overall power requirement recorded in August was mainly due to a severe propeller fouling. This is confirmed by a cross-comparison between all KPIs. Those including both effects of hull

and propeller fouling ($\widehat{P_K}, \widehat{w_K}$ and ϕ) show a small increase from July to August. ΔC_f, which virtually only includes the effects of propeller fouling, doesn't show an appreciable change from July to August. This confirms that hull fouling had not changed significantly its impact.

Considering the fouling state of the R/V hull, the estimation of viscous drag increase and ΔC_f seem very reasonable. The significance of this value could be further confirmed by service monitoring or trials immediately following a dry-dock.

On these grounds, the changes in the KPIs observed thus far must be attributed to both an increase in hull and propeller surface roughness. In a much lesser extent, the effects of disturbances that could not be entirely corrected contribute to the scatter in the KPIs. For all KPIs, an increase is observed within expectations, suggesting that in spite of the weather-induced noise the methodology is correct and bodes well for a longer-term analysis of fouling.

4 Conclusions

A deterministic ship performance monitoring system (SPMS) dedicated to the analysis of biofouling growth on hull and propeller was developed. Its founding methodology and principles were here detailed in the attempt to provide a useful method to estimate the biofouling effect on ship performance and to aid the selection of fouling control coating systems. The benefits of the deterministic approach against other available methods were discussed.

An equation to define the time constant ϵ for the timing of data analysis was suggested and it was found that for *The Princess Royal* $\epsilon = 23$s. A symmetric 5% trimmed standard deviation and the generalised Extreme Studentised Deviate were

suggested to identify respectively steady-state periods and outliers when preparing raw data for the analysis.

The full-scale measurements and monitoring onboard *The Princess Royal* proved consistent with the expectations and gave promising results, suggesting that the methodology presented in this paper is correct. From the baseline generated on the 14th November, a maximum increase in the total resistance of about 21% was observed at the higher F_n, corresponding to an estimated 69% increase in viscous drag and a 37% wake fraction gain. An average $\Delta C_f = 2 \times 10^{-3}$ could also be estimated from the service performance analysis. These estimations appear very much in line with estimations in the literature for comparable hull fouling coverages, eg [1].

It was also demonstrated how the ship service performance analysis largely benefits from the use of multiple KPIs to validate and strengthen the evaluation of the effects of fouling. A larger data set would undoubtedly improve the reliability of the KPIs, which could thereafter be employed alongside bottom-up approaches (e.g. [58]) for the estimation of biofouling effect. The implementation of a similar SPMS on larger vessels would, also, reduce the data noise because of the lesser relative impact of disturbances. On a side note, full-scale thrust measurements were confirmed to be the least stable and reliable in this SPMS. More advanced thrust measurements systems do exist, and their installation is recommended in virtue of the valuable information they would provide.

5 Acknowledgements

The Authors are grateful to Dr. Serena Lim of Newcastle University for her support in organising and conducting the sea trials onboard *The Princess Royal*. The Authors thank the Sasaki-SMP fund, by which this project was supported. Finally, the Authors also acknowledge

the support given by International Paint throughout the development of the SPMS and for the supply of test paint and one of the two instrumented shafts.

References

[1] Schultz, M. P. (2007), `Effects of coating roughness and biofouling on ship resistance and powering', Biofouling 23(5), 331341.

[2] Telfer, E. V. (1926), `The Practical Analysis of Merchant Ship Trials and Service Performance', Trans. North East Coast Institution of Engineers and Shipbuilders (NECIES) 43, 6398.

[3] EC (2015), `On the monitoring, reporting and verification of carbon dioxide emissions from maritime transport, and amending Directive 2009/16/EC'.

[4] EC (2016), `On determination of cargo carried for categories of ships other than passenger, ro-ro and container ships pursuant to Regulation (EU) 2015/757 of the European Parliament and of the Council on the monitoring, reporting and verification of carbon dioxide emissions from maritime transport'.

[5] Yebra, D. M., Kiil, S. and Dam-Johansen, K. (2004), `Antifouling technology past, present and future steps towards efficient and environmentally friendly antifouling coatings', Progress in Organic Coatings 50(2), 75104.

[6] Yeginbayeva, I. A. (2017), An investigation into hydrodynamic performance of marine coatings "in-service" conditions, PhD Thesis, Newcastle University, Newcastle upon Tyne, UK.

[7] ISO (2016), Measurement of changes in hull and propeller performance, International Standard 19030, International Standardization Organization.

[8] ITTC (2014), Analysis of Speed/Power Trial Data, Recommended Procedures and Guidelines 7.5-04-01-01.2, International Towing Tank Conference.

[9] Haslbeck, E. G. and Bohlander, G. S. (1992), Microbial biofilm effects on drag - Lab and field, in `Proc. of the Ship Production Symposium', SNAME, New Orleans, US.

[10] Hunsucker, J. T. (2016), Quantification of frictional drag due to biofouling on in-service ships, PhD Thesis, Florida Institute of Technology, Melbourne, US.

[11] Hasselaar, T. W. (2011), An investigation into the development of an advanced ship performance monitoring and analysis system, PhD Thesis, Newcastle University, Newcastle upon Tyne, UK.

[12] Logan, K. P. (2011), Using a Ship's Propeller for Hull Condition Monitoring, in `Proc. of the ASNE Intelligent Ships Symposium IX', Philadelphia, US.

[13] Orihara, H. and Tsujimoto, M. (2017), `Performance prediction of full-scale ship and analysis by means of on-board monitoring. Part 2: Validation of full-scale performance predictions in actual seas', Journal of Marine Science and Technology.

[14] Petersen, J. P., Jacobsen, D. J. and Winther, O. (2012), `Statistical modelling for ship propulsion efficiency', Journal of Marine Science and Technology 17(1), 3039.

[15] Pedersen, B. P. and Larsen, J. (2013), Gaussian Process Regression for Vessel Performance Monitoring, in `Proc. of the 12th International Conference on Computer and Applications in the Maritime Industries (COMPIT 13)', Cortona, IT.

[16] Haranen, M., Pakkanen, P., Kariranta, R. and Salo, J. (2016), White, Grey and Black-Box Modelling in Ship Performance Evaluation, in `Proc. of the 1st Hull Performance and Insight Conference (HullPIC '16)', Castello di Pavone, IT.

[17] Maki, A., Akimoto, Y., Nagata, Y., Kobayashi, S., Kobayashi, E., Shiotani, S., Ohsawa, T. and Umeda, N. (2011), `A new weather-routing system that accounts for ship stability based on a real-coded genetic algorithm', Journal of Marine Science and Technology 16(3), 311322.

[18] Coraddu, A., Oneto, L., Baldi, F. and Anguita, D. (2017), `Vessel fuel consumption forecast and trim optimization: A data analytics perspective', Ocean Engineering 130.

[19] Reid, R. E. (1985), `A Condition and Performance Monitoring System with Application to U.S. Navy Ship Operations', Naval Engineers Journal 97(7), 2938.

[20] Leifsson, L. ., Sævarsdóttir, H., Sigurðsson, S. . and Vésteinsson, A. (2008), `Grey-box modeling of an ocean vessel for operational optimization', Simulation Modelling Practice and Theory 16(8), 923932.

[21] Munk, T. and Kane, D. (2011), Technical fuel conservation policy and Hull and Propeller Performance, in `Proc. of the International Conference on Design and Operation of Tankers', Royal Institution of Naval Architects, Athens, GR.

[22] Solonen, A. (2016), Experiences with ISO-19030 and Beyond, in `Proc. of the 1st Hull Performance and Insight Conference (HullPIC '16)', Castello di Pavone, IT.

[23] Carchen, A., Sasaki, N., Aktas, B., Turkmen, S. and Atlar, M. (2015), Design and review of the new `NPT' propeller for The Princess Royal, in `Proc. of the 4th International Conference on Advanced Model Measurement Technology for The Maritime Industry (AMT'15)', Istanbul, TR.

[24] Atlar, M., Yeginbayeva, I. A., Turkmen, S., Demirel, Y. K., Carchen, A., Marino, A. and Williams, D. (2018), A rational approach to predicting the effect of antifouling systems on “in-service” ship performance, in `Proc. of the 3rd International Symposium on Naval Architecture and Maritime', Istanbul, TR.

[25] Blok, J. J. (1993), The Resistance Increase of a Ship in Waves, PhD Thesis, Technische Universiteit Delft, Delft, NL.

[26] Taskar, B., Yum, K. K., Steen, S. and Pedersen, E. (2016), `The effect of waves on engine-propeller dynamics and propulsion performance of ships', Ocean Engineering 122, 262277.

[27] Bhattacharyya, R. (1978), Dynamics of marine vehicles, Wiley, NY.

[28] van den Boom, H., Huisman, H. and Mennen, F. (2015), `New Guidelines for Speed/Power Trials'.

[29] Bertram, V. (2016), Added Power in Waves - Time to Stop Lying (to Ourselves), in `Proc. of the 1st Hull Performance and Insight Conference (HullPIC '16)', Castello di Pavone, IT.

[30] Faltinsen, O., Zhao, R. and Umeda, N. (1991), `Numerical Predictions of Ship Motions at High Forward Speed', Philosophical Transactions of the Royal Society A: Mathematical, Physical and Engineering Sciences 334(1634), 241252.

[31] Sfakianos, N. (2016), Prediction of Added Wave Resistance of Princess Royal Research Vessel using model tests, Master's thesis, Newcastle University, Newcastle upon Tyne, UK.

[32] Aage, C. (1971), Wind coefficients for nine ship models, Technical Report No. A-3, Hydro-og Aerodynamisk Laboratorium, Lyngby, DK.

[33] Blendermann, W. (1996), Wind Loading of Ships - Collected Data from Wind Tunnel Tests in Uniform Flow, Technical Report 574, Institut für Schibau der Universität Hamburg, Hamburg, DE.

[34] van den Boom, H. J. and Hasselaar, T. W. (2014), Ship Speed-Power Performance Assessment, in `Proc. of the SNAME Annual Meeting', SNAME.

[35] Vranakis, E., Axiotis, D., Carchen, A., Trodden, D. and Atlar, M. (2017), Investigation into the wind loadings applied to a deep-v catamaran using experimental and numerical approaches, in `Proc. of the 5th International Conference on Advanced Model Measurement Technology for The Maritime Industry (AMT'17)', Glasgow, UK.

[36] Yasukawa, H. and Yoshimura, Y. (2015), `Introduction of MMG standard method for ship maneuvering predictions', Journal of Marine Science and Technology 20, 3752.

[37] Carchen, A., Shi, W., Sasaki, N. and Atlar, M. (2016), A prediction program of manoeuvrability for a ship with a Gate Rudder system, in `Proc. of the 2nd International `A. Yücel Odaba³' Colloquium', A. Yücel Odaba³Colloquium series, Istanbul, TR.

[38] Yasukawa, H. (1992), `Hydrodynamic interactions among hull, rudder and propeller of a turning thin ship', Trans. West-Japan Society of Naval Architects (84), 5983.

[39] Lackenby, H. (1963), `The Effect of Shallow Water on Ship Speed', The Shipbuilder and the Marine Engine-Builder 70(672).

[40] Raven, H. C. (2016), A new correction for Shallow-Water effects in ship Speed Trials, in `Proc. of the 13th International Symposium on PRActical Design of Ships and Other Floating Structures (PRADS 2016)', Copenhagen, DK.

[41] ITTC (1966), Report of the Performance Committee, in `Proc. of ITTC '66', Tokyo, JP.

[42] Atlar, M., Aktas, B., Sampson, R., Seo, K.-C., Viola, I. M., Fitzsimmons, P. and Fetherstonhaugh, C. (2013), A multipurpose marine science and technology research vessel for full-scale observations and measurements, in `Proc. of the 3rd International Conference on Advanced Model Measurement Technology for The Maritime Industry (AMT'13)', Gdansk, PL.

[43] Mosaad, M. A. (1986), Marine Propeller Roughness Penalties, PhD Thesis, Newcastle University, Newcastle upon Tyne, UK.

[44] Aldous, L., Smith, T. and Bucknall, R. (2013), Noon report Data Uncertainty, in `Proc. of the Low Carbon Shipping and Shipping in Changing Climates Conference (LCS 2013)', London, UK.

[45] Aldous, L., Smith, T., Bucknall, R. and Thompson, P. (2015), `Uncertainty Analysis in ship performance monitoring', Ocean Engineering 110, 2938.

[46] Dückert, T., Schmode, D. and Tullberg, M. (2016), Computing Hull and Propeller Performance: Ship Model Alternatives and Data Acquisition Methods, in `Proc. of the 1st Hull Performance and Insight Conference (HullPIC '16)', Castello di Pavone, IT.

[47] Antola, M., Solonen, A. and Straboulis, S. (2017), The Art of Scarcity: Combining High-Frequency Data with Noon Reports in Ship Modeling, in `Proc. of the 2nd Hull Performance and Insight Conference (HullPIC '17)', Ulrichshusen, DE.

[48] IMO (2002), `Guidelines on Voyage Data Recorder (VDR) ownership and recovery'.

[49] Moat, B. I., Yelland, M. J., Pascal, R. W. and Molland, A. F. (2006a), `Quantifying the Airflow Distortion over Merchant Ships. Part I: Validation of a CFD Model', Journal of Atmospheric and Ocean Technology 23.

[50] Moat, B. I., Yelland, M. J., Pascal, R. W. and Molland, A. F. (2006b), `Quantifying the Airflow Distortion over Merchant Ships. Part II: Application of the Model Results', Journal of Atmospheric and Ocean Technology 23.

[51] Crowe, E. L., Davis, F. A. and Maxeld, M. W. (1955), Statistics Manual, Dover Publications, New York, US.

[52] Barnett, V. and Lewis, T. (1994), Outliers in Statistical Data, Wiley, UK.

[53] Atlar, M., Glover, E. J., Candries, M., Mutton, R. and Anderson, C. D. (2002), The effect of a Foul Release coating on propeller performance, in `Proc. of the 2nd International Conference on Marine Science and Technology for Environmental Sustainability (ENSUS2001)', Newcastle upon Tyne, UK.

[54] Seo, K.-C., Atlar, M. and Goo, B. (2016), `A Study on the Hydrodynamic Effect of Biofouling on Marine Propeller', Journal of the Korean Society of Marine Environment and Safety 22(1), 123 128.

[55] Molland, A. F., Wellicome, J. F. and Couser, P. R. (1994), Resistance experiments on a systematic series of high-speed displacement catamaran forms: variation of length-displacement ratio and breadth-draught ratio, Technical Report 71, University of Southampton, Southampton, UK.

[56] ITTC (2011), 1978 ITTC Performance Prediction Method, Recommended Procedures and Guidelines 7.5-02-03-01.4, International Towing Tank Conference.

[57] Carchen, A., Turkmen, S., Pazouki, K., Murphy, A., Aktas, B. and Atlar, M. (2017), Uncertainty Analysis of full-scale ship performance monitoring onboard The Princess Royal, in `Proc. of the 5th International Conference on Advanced Model Measurement Technology for The Maritime Industry (AMT'17)', Glasgow, UK.

[58] Demirel, Y. K., Uzun, D., Zhang, Y., Fang, H.-C., Day, A. H. and Turan, O. (2017), `Effect of barnacle fouling on ship resistance and powering', Biofouling 33(10), 819834.

Length Overall [L_{oa}]	18.88 m
Length B.P. [L_{pp}]	16.45 m
Beam, moulded [B]	7.3 m
Displacement [Δ]	45.5 t
Average midship draft [T]	1.86 m
Wetted surface [S]	118.52 m^2
Block Coefficient [C_b]	0.362
Max. Speed [V_s]	22 kn
Propeller diameter [D_p]	0.75 m

Table 1. *The Princess Royal* main characteristics.

Sensor	**Location**	**Sampling frequency**
DGPS and Gyrocompass	Mast	1 Hz
Doppler Speed Log	Hull bottom at $L_{pp}/2$	1 Hz
Instrumented shafts	Abaft the gearboxes	2 Hz
Electro-Magnetic Speed Log	Outer hull plating on the forebody	1 Hz
Rudder potentiometer	Rudder stock	1 Hz
Weather station (ultrasonic anemometer)	Mast top	0.3 Hz
Wave radar	Bow gunwale	2.6 Hz
Wave buoy	Newbiggin	$5.5*10^{-4}$ Hz
Thermosalinograph	Sea chest on the bottom plating	16 Hz

Table 2. Summary of the sensors used in the monitoring system on board *The Princess Royal*.

Variable	Symbol	Reliability
Time	s	• • •
Speed Over Ground	V_g	• • •
Course Over Ground	ψ_g	• • •
Heading	ψ	• • •
Speed Through Water	u	••
Propeller speed	n	• • •
Propeller Torque	Q_p	••
Propeller Thrust	T_p	•
Rudder angle	δ	• • •
Wind speed	V_{AAR}	••
Wind direction	ψ_{AAR}	••
Wave amplitude	ζ	••
Wave spectrum	S_ζ	••
Water properties	ρ, ν	••

Table 3. Summary of the measured variables and indicative reliability.

V_s	5%
RPM	1%
Q_p	1%
ψ	2

Table 4. Allowed steady-state variability.

Appendix A

In the following, the derivation of the time constant ϵ is detailed. The single degree-of-freedom motion equation dependent on time t for a vessel is:

$$(1 - t_d)T_p(t) - R_T(t) = \Delta(1 + m_x)\frac{\mathrm{d}u}{\mathrm{d}t} \tag{A.1}$$

where t_d is the thrust deduction factor, T_p the propeller thrust, R_T the total ship resistance, Δ the ship mass displacement, m_x the nondimensional added mass in surge direction and u the forward component of the speed through the water. Defining the functions:

$$\mathrm{a}(t) = \frac{T_p(t)}{\tilde{T}_p}; \quad \mathrm{b}(t) = \frac{R_T(t)}{\tilde{R}_T}; \quad \mathrm{c}(t) = \frac{u(t)}{\tilde{V}_s}; \tag{A.2}$$

where $\tilde{T}_p$ and $\tilde{R}_T$ are the thrust and the resistance at the design ship speed the through water $\tilde{V}_s$ and replacing eq. (2) into eq. (A.1) yields:

$$\frac{\tilde{P}_s\,\eta_D\,\eta_s}{\tilde{V}_s}\left[\frac{\mathrm{a}(t)-\mathrm{b}(t)}{\mathrm{c}(t)}\right] \approx \Delta(1 + m_x)\tilde{V}_s\frac{\mathrm{d}c(t)}{\mathrm{d}t} \tag{A.3}$$

$$\therefore \int_0^{\epsilon} dt \approx \frac{\tilde{V}_s^2\Delta}{\tilde{P}_s\kappa}\int_0^{\epsilon}\left[\frac{\mathrm{c}(t)}{\mathrm{a}(t) - \mathrm{b}(t)}\right]\frac{dc(t)}{dt}dt$$

$$\therefore\ \epsilon \approx \frac{\tilde{V}_s^2\Delta}{\tilde{P}_s k_t}\int_{c_{\mathrm{ini}}}^{c_{\mathrm{fin}}}\left[\frac{\mathrm{c}}{\mathrm{a}(\mathrm{c}) - \mathrm{b}(\mathrm{c})}\right]dc$$

Where:

$$\eta_D = \eta_0\eta_r\left(\frac{1-t_d}{1-w}\right); \quad k_t = \frac{\eta_D\eta_s}{(1+m_x)}; \tag{A.4}$$

c_{ini} and c_{fin} are respectively the initial and final nondimensional velocities over which to integrate the time. The parameter $\xi = \tilde{V}_s^2\Delta/\tilde{P}_s k_t$ has the dimension of seconds. The

desired time would be long enough to encompass the slowest accelerations, which occurs when both c_{ini} and c_{fin} are small. It is suggested that:

$$c_{\text{ini}} = 0\,\text{kn}; \quad c_{\text{fin}} = c\left(0.1\tilde{P}_s\right)$$

which corresponds to a power increase of $10\%\widetilde{P_s}$ from idle. The asymptotic behaviour of $\mathrm{c}(t)$ was considered to converge when it reached within $0.01\mathrm{c}_{\text{fin}}$. The function t in these terms was studied with a manoeuvrability simulator for three different vessel types, namely a small high-speed vessel, a medium-sized chemical tanker and a VLCC. Results are shown in Table A.1. Defining ϵ as a function of ξ yielded:

$$\epsilon = \frac{7941\,\xi}{2724+\xi} \tag{A.5}$$

k_t may be taken as 0.55 considering $\eta_D = 0.6$ and $(1 + m_x) = 1.08$.

Table A.1: Simulated time constant values.

Vessel type	$\boldsymbol{\epsilon}$
High speed vessel	21s
Small tanker	619s
VLCC	3444s

Appendix B

Figure B.1. Validation of σ_{AW} transfer function by means of towing tank tests.

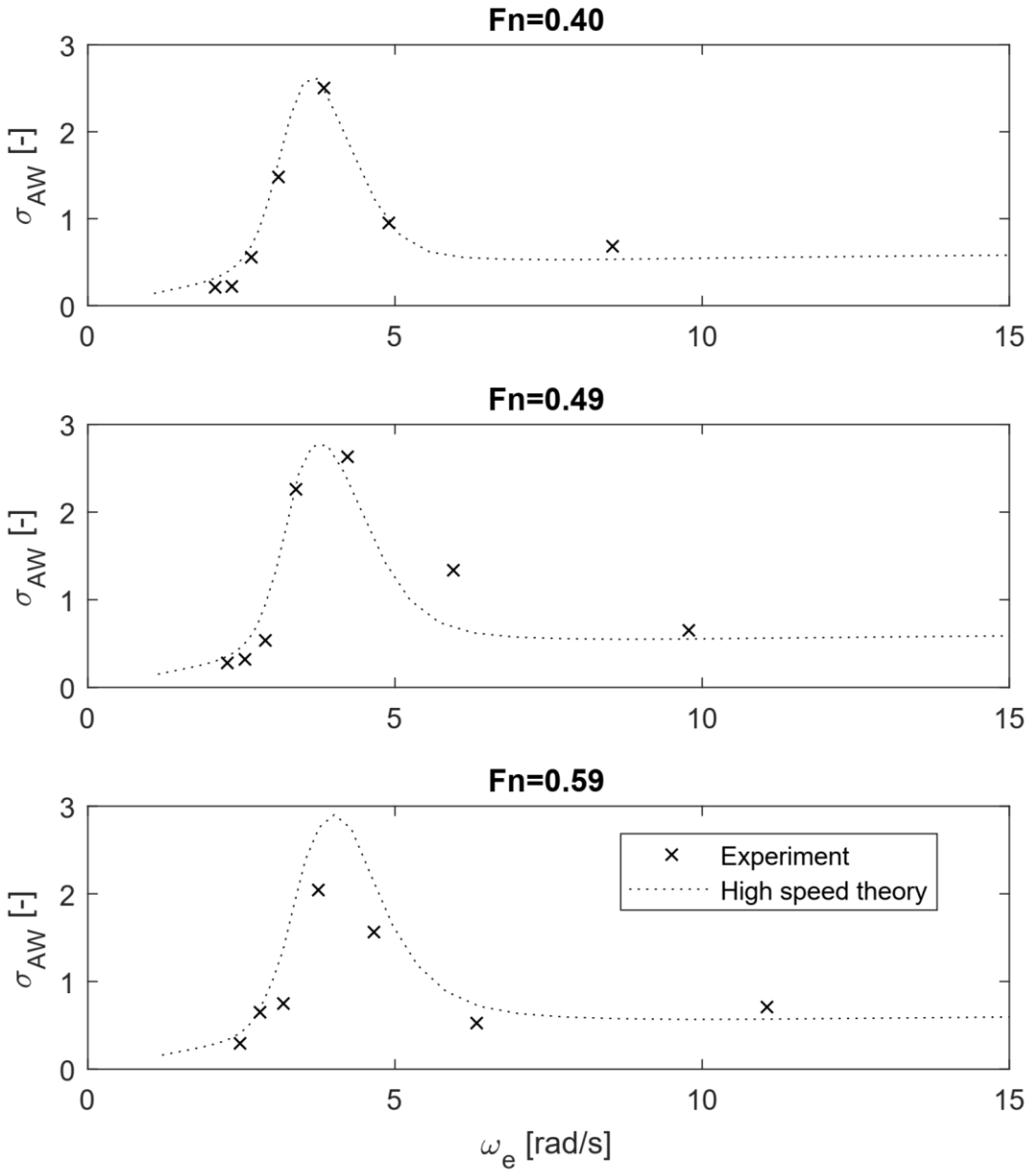

Figure B.2. Total added resistance, R_{add}, for all performance trials and monitoring.

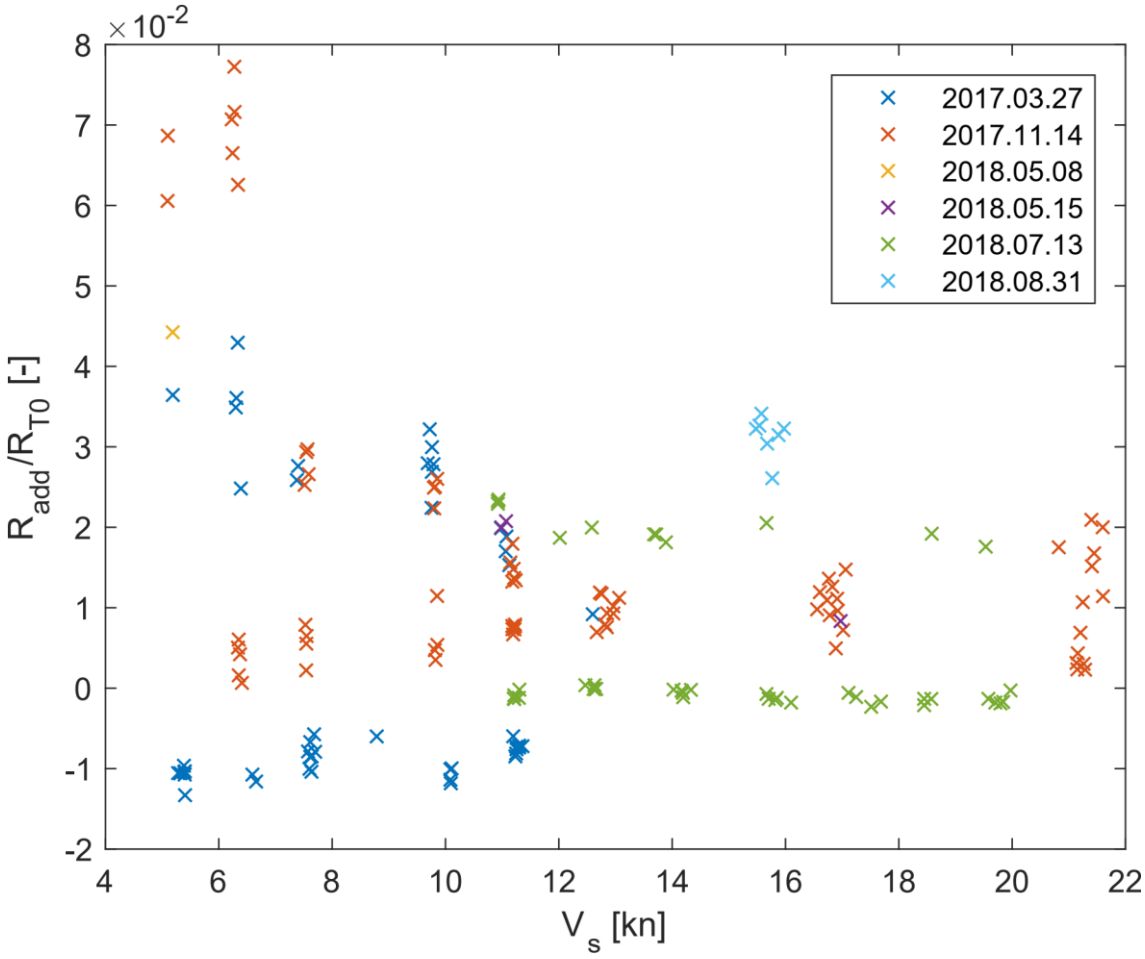

Figure B.3. Satellite view of the trial location.

Figure B.4. Port propeller fouling photographed during an underwater survey in July 2018.

Figure B.5. Normalised delivered power for all performance trials and monitoring.

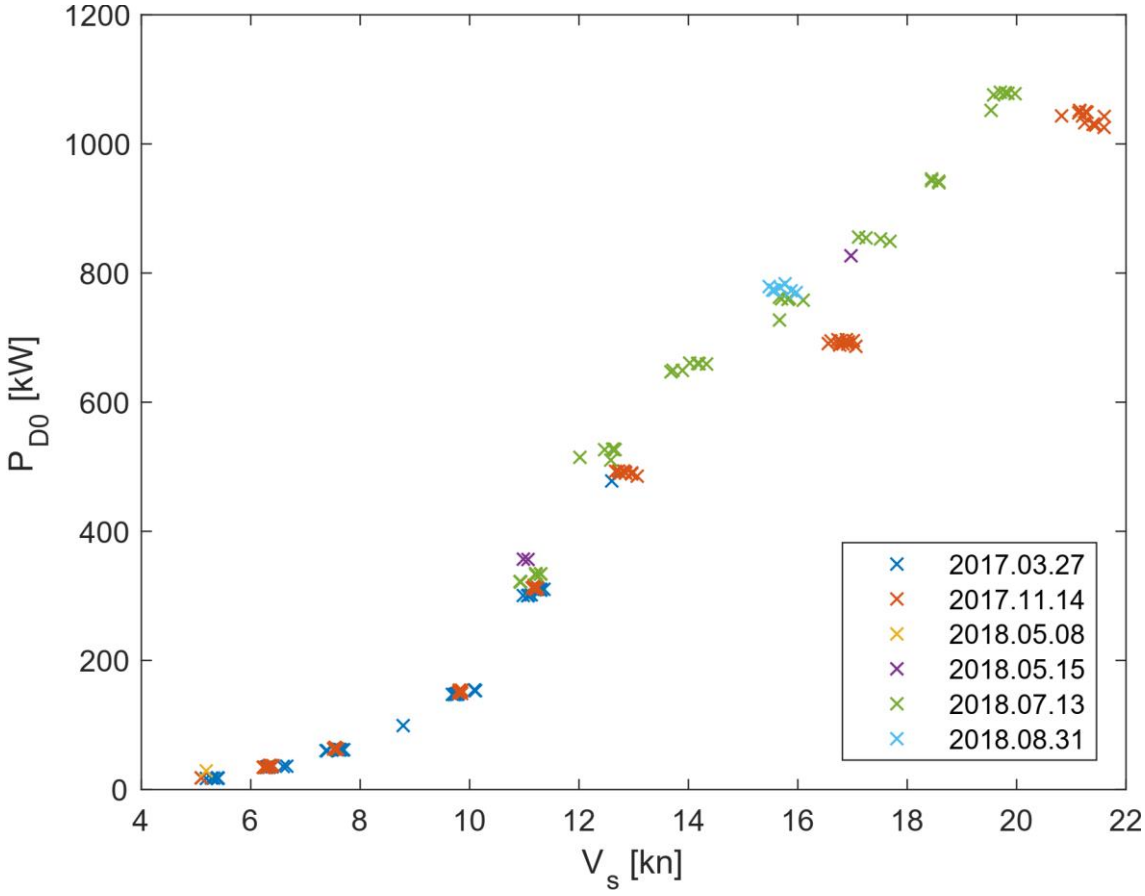
1200
1000
800
600
400
200
0
P_{D0} [kW]
4
6
8
10
12
14
16
18
20
22
V_s [kn]
2017.03.27
2017.11.14
2018.05.08
2018.05.15
2018.07.13
2018.08.31